

TSCAN: Context-Aware Uplift Modeling via Two-Stage Training for Online Merchant Business Diagnosis

HANGTAO ZHANG, Rajax Network Technology (ele.me), China

ZHE LI, Rajax Network Technology (ele.me), China

KAIRUI ZHANG, Rajax Network Technology (ele.me), China

Estimating Individual Treatment Effect (ITE) is crucial for business diagnosis in the online food ordering industry, particularly for assessing the impact of various business strategies, such as inventory management, pricing optimization, online marketing campaigns, product launches, on merchant revenue. A primary challenge in ITE estimation is sample selection bias. Traditional approaches utilize treatment regularization techniques such as the Integral Probability Metrics (IPM), re-weighting, and propensity score modeling to mitigate this bias. However, these regularizations may introduce undesirable information loss and limit the performance of the model. Furthermore, treatment effects vary across different external contexts, and the existing methods are insufficient in fully interacting with and utilizing these contextual features. To address these issues, we propose a Context-Aware uplift model based on the Two-Stage training approach (TSCAN), comprising CAN-U and CAN-D sub-models. In the first stage, we train an uplift model, called CAN-U, which includes the treatment regularizations of IPM and propensity score prediction, to generate a complete dataset with counterfactual uplift labels. In the second stage, we train a model named CAN-D, which utilizes an isotonic output layer to directly model uplift effects, thereby eliminating the reliance on the regularization components. CAN-D adaptively corrects the errors estimated by CAN-U through reinforcing the factual samples, while avoiding the negative impacts associated with the aforementioned regularizations. Additionally, we introduce a Context-Aware Attention Layer throughout the two-stage process to manage the interactions between treatment, merchant, and contextual features, thereby modeling the varying treatment effect in different contexts. We conduct extensive experiments on two real-world datasets to validate the effectiveness of TSCAN. Ultimately, the deployment of our model for real-world merchant diagnosis on one of China's largest online food ordering platforms validates its practical utility and impact.

Additional Key Words and Phrases: Uplift modeling, Two-Stage training, Context-Aware interaction

ACM Reference Format:

Hangtao Zhang, Zhe Li, and Kairui Zhang. 2025. TSCAN: Context-Aware Uplift Modeling via Two-Stage Training for Online Merchant Business Diagnosis. 1, 1 (April 2025), 15 pages. <https://doi.org/XXXXXXX.XXXXXX>

1 Introduction

In recent years, the e-commerce sector, particularly the food ordering industry, has seen rapid growth, with China emerging as the largest market, boasting a size of US \$46.6 billion in 2023 [1]. This growth has prompted an increasing number of independent merchants to shift towards online sales [2]. However, many of these merchants lack sufficient experience in online operations, making

Authors' Contact Information: Hangtao Zhang, zht267501@alibaba-inc.com, Rajax Network Technology (ele.me), Hangzhou, China; Zhe Li, lz171761@alibaba-inc.com, Rajax Network Technology (ele.me), Shanghai, China; Kairui Zhang, kairui.zhang@alibaba-inc.com, Rajax Network Technology (ele.me), Shanghai, China.

Permission to make digital or hard copies of all or part of this work for personal or classroom use is granted without fee provided that copies are not made or distributed for profit or commercial advantage and that copies bear this notice and the full citation on the first page. Copyrights for components of this work owned by others than the author(s) must be honored. Abstracting with credit is permitted. To copy otherwise, or republish, to post on servers or to redistribute to lists, requires prior specific permission and/or a fee. Request permissions from permissions@acm.org.

© 2025 Copyright held by the owner/author(s). Publication rights licensed to ACM.

ACM XXXX-XXXX/2025/4-ART

<https://doi.org/XXXXXXX.XXXXXX>

it challenging for them to navigate the complex management processes and diverse marketing tools available [3]. To assist these merchants in accurately identifying business issues and delivering personalized solutions, it is crucial to assess the impact of each diagnostic on their operations. This problem differs from traditional supervised learning tasks as it fundamentally involves causal inference. In real-world scenarios, we typically only observe a merchant's response to a specific marketing strategy (i.e., whether they participated a particular marketing activity or not), but rarely observe their performance under both participating and non-participating strategies simultaneously. To address this problem, researchers have developed methods for modeling individual uplift, known as Individual Treatment Effect (ITE) Estimation [4, 5]. These techniques are primarily used to evaluate the magnitude of the response to an intervention (treatment) across different individuals. The main ITE estimation methods include [6–8]: Meta-Learning Methods (e.g., S-Learning[9], T-Learning[9], X-Learning[9]), Tree-based Methods (e.g., BART[10], CausalForest[11]), and Deep Learning Methods (e.g., TransTEE[6], CEVAE[12], CFR-ISW[13]). Recent research trends indicate that deep learning-based methods are gaining popularity due to their powerful non-linear representation and feature interaction capabilities[6, 8, 13–15]. These deep learning models can be further categorized into[8]:

- Balanced Representation Learning (e.g., BNN[16], TransTEE).
- Covariate Confounding Learning (e.g., CEVAE, Dragonnet[17]).
- Adversarial Generative Network Models (e.g., CEGAN[18], GANITE[19], SCIGAN[20]).

These methods employ various techniques to mitigate sample selection bias and negative impacts of confounding factors. For instance, Balanced Representation Learning primarily uses Integral Probability Metric (IPM) loss to reduce the discrepancy between the distributions of positive samples $p(\Phi(x)|t = 0)$ and negative samples $p(\Phi(x)|t = 1)$ [21, 22]. Additionally, CFR-ISW enhances this approach by incorporating a re-weighting strategy, in which the sample weight is related to propensity score. Methods based on covariate confounding learning primarily encode both observed and unobserved confounders using approaches such as autoencoders or propensity score prediction networks, thereby eliminating the influence of these confounding factors [23–25]. However, despite the promising results in ITE estimation methods, many branch-structured neural network models and meta-learning methods are still unable to handle continuous treatments directly. Moreover, most methods inevitably introduce additional errors to reduce the negative impact of sample selection bias [26]. For example, it is widely acknowledged that excessive enforcement of balance can be detrimental, as it may unintentionally eliminate information that is predictive of outcomes [26, 27]. The re-weighting strategy also alters the original distribution of the samples, thereby amplifying the impact of long-tail samples [28]. Incorporating a propensity score prediction task will also affect the prediction of outcome. This is evidenced in the fact that, when training under the same conditions, ablating these regularizations can improve the prediction accuracy of practical samples. Additionally, most existing models lack exploration of the treatment information representation in different contexts. In online marketing, the impact of treatments on merchant sales is significantly influenced by market dynamics. For example, in a high-demand market, consumers may be less sensitive to merchant subsidies, whereas users may exhibit higher sensitivity in a market with abundant choices. Similarly, in ad bidding, the same ad bid (treatment) can have varying effects depending on competitor bids (context). We refer to this as contextual information, and it is crucial for uplift estimates. However, we observe that almost all existing methods do not fully leverage this contextual information, potentially impacting the accuracy of uplift estimation. We term this challenge as the underutilization of contextual features. In summary, the primary challenges are: (1) developing more effective methods to address selection bias while maintaining the predictive

performance of the model and the quality of personalized recommendations; (2) inadequately considering the impact of contextual factors on treatment effects.

To this end, we propose a Context-Aware uplift model based on a Two-Stage training approach (TSCAN). TSCAN includes two sub-models: CAN-U and CAN-D. CAN-U is designed with the treatment regularizations of IPM loss term and propensity score module to address sample selection bias and effectively capture treatment effects. Then CAN-U generates the uplift value \hat{u} , defined as $\hat{u} = \hat{y}(t = t_f) - \hat{y}(t = t_{cf})$, during the sampling of counterfactual treatment, in which \hat{y} represents the predicted outcome, with t_f and t_{cf} denote factual and counterfactual treatment values, respectively. These attempts subject \hat{u} to the errors caused by treatment regularizations. Therefore, in the second stage, we combine factual data with the generated uplift \hat{u} into a complete dataset to train a new model, called CAN-D, for directly estimating treatment effects in a supervised manner. It is essential to highlight several critical points about CAN-D. First, CAN-D can adaptively correct the uplift predicted by CAN-U through utilizing factual data. Second, CAN-D avoids the associated information loss and the additional prediction errors by eliminating IPM and propensity score regularizations. Third, CAN-D employs an isotonic output layer to capture the monotonic relationships between the treatment context and the estimated treatment effects. This design ensures that the predictions remain consistent with the underlying casual structures, enhancing both interpretability and reliability, which are particularly crucial for gaining the trust of business owners in diagnostic applications. Additionally, in both CAN-U and CAN-D, the Context-Aware Attention layer is designed to capture interactions between treatment and merchant features, as well as contextual information, enabling the modeling of diverse treatment effect patterns across various contexts. Finally, comprehensive experiments on two benchmarks with seven baselines are conducted, which show the effectiveness of our TSCAN model.

2 RELATED WORK

In this section, we provide a concise overview of the primary existing works on uplift models and feature interaction methods.

2.1 Uplift Model

Over the past few decades, causal inference has seen extensive application and development across various fields, including computer science, medicine, economics, and education[29–31]. The primary methods for predicting ITE include: (1) meta-learning methods (e.g., S-Learning, T-Learning, X-Learning); (2) tree-based methods (e.g., BART, CausalForest); and (3) deep learning methods (e.g., TransTEE, CEVAE, CFR-ISW). Recently, deep causal models have gained significant attention and have become the core tools for unbiased estimation of treatment effects [6, 8, 14, 32, 33]. These deep causal models can be further categorized based on different techniques and applications[8], such as (1)learning balanced representations (e.g., BNN, TransTEE), (2)covariate confounding learning (e.g., CEVAE, Dragonnet), and (3) Generative Adversarial Networks (GANs)-based counterfactual simulation (e.g., CEGAN, SCIGAN). However, these existing technologies may introduce information loss and errors when addressing confounder bias, and the training process of the GAN model is often unstable[26–28]. Additionally, most methods do not directly model the uplift but instead make predictions on the same sample under different treatments and calculate the difference as the uplift. Our proposed TSCAN model and its training process differ from the existing approaches. The development of TSCAN aims to eliminate the errors caused by regularizations used for ITE estimation, thereby improving the ITE prediction accuracy.

2.2 Feature Interaction

Sufficient feature interaction can enhance model performance[34–36]. TransTEE integrates semantic and quantitative information about treatments to facilitate continuous treatment effect estimation. EFIN proposes a treatment-aware interaction module that models the interactions between treatment features and other factors, capturing the degree to which different treatments motivate customers. However, current research has not explicitly considered the interaction of external contextual factors (beyond just treatment and individual characteristics) on treatment effects. To address this issue, we propose a Context-Aware Attention Layer that seeks to integrate context features with both treatment and individual (merchant) characteristics, thereby modeling the extent to which treatments motivate individuals in different contexts.

3 PRELIMINARIES

In the scenario of estimating treatment effects for business diagnosis in the online food ordering industry, our goal is to estimate the ITE using the observed data $D = \{(X_i, t_i, y_i)\}_{i=1}^N$, where X_i , t_i , and y_i represent the merchant shop (referred to as "merchant" for brevity) feature vector, treatment feature, and outcome vector, respectively. The treatment variable t_i can be binary, indicating whether a merchant has initiated a marketing activity (i.e., $t_i \in \{0, 1\}$), or continuous, such as the number of customers reviews (i.e., $t_i \in \mathbb{R}$). The outcome variable y_i is continuous, representing the merchant's order count or revenue (i.e., $y_i \in \mathbb{R}$). The sample size is denoted by N . The potential outcome of the i -th instance under treatment value k is denoted as $y_i(t_i = k)$, and the conditional probability of assigning treatment k given features X_i is expressed as $\pi(X_i, k) = P(t_i = k | X_i)$, commonly referred to as the propensity score. In observational data, we can typically observe the outcome values under a specific treatment rather than under all possible treatments. This limitation distinguishes uplift modeling from traditional supervised learning. Uplift modeling seeks to accurately estimate the expected outcome for each instance across different treatments:

$$\tau(X_i, k_1, k_0) = E(y_i(t = k_1) - y_i(t = k_0)) \quad (1)$$

$$= E(y_i(k_1)|t_i = k_1, X_i) - E(y_i(k_0)|t_i = k_0, X_i) \quad (2)$$

4 THE PROPOSED METHOD

As described in Section 1, existing methods encounter the following challenges: (1) a decline in both model prediction performance and personalized recommendation capabilities, caused by treatment regularizations; (2) insufficient consideration of contextual factors in estimating treatment effects.

In this section, we propose the TSCAN model along with a two-stage training strategy to address the aforementioned challenges. TSCAN contains two sub-models: CAN-U and CAN-D. The former incorporates an IPM loss term and a propensity score prediction module as treatment regularizations, aiming to minimize sample selection bias and accurately capture causal relationships. Instead of generating counterfactual samples through GANs, we utilize the enhanced ITE prediction model CAN-U to generate the pseudo uplift label \tilde{u} for each sample. Then we get a complete dataset $\tilde{D} = (X, t_f, y_f, t_{cf}, \tilde{u})$, in which y_f is the factual outcome label. In the second stage, we develop the CAN-D model, which removes the treatment regularizations and uses an isotonic output layer to directly model the uplift values on \tilde{D} . The CAN-D model is trained to adaptively correct the errors estimated by CAN-U through reinforcing factual samples. The training process is illustrated in Figure 1.

4.1 Training

In this section we describe the TSCAN model training process in detail:

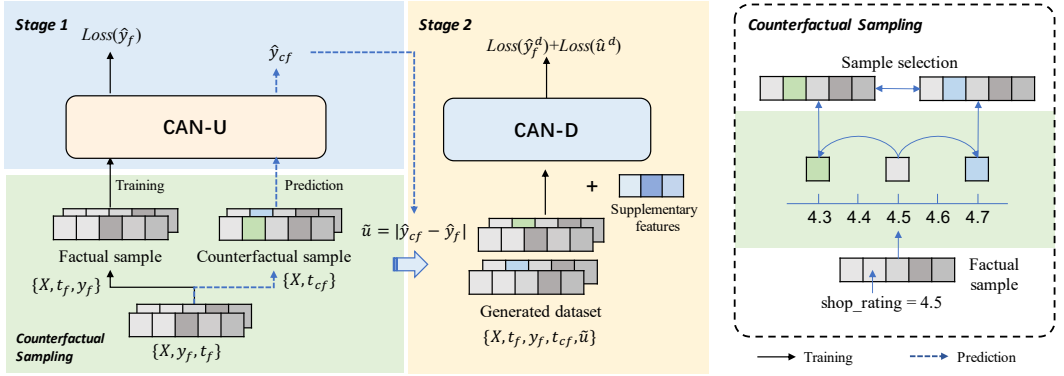


Fig. 1. Diagram illustrating TSCAN's two-stage training process and counterfactual sampling diagram, where the black solid line representing the training flow and the blue dotted line representing the prediction flow.

Stage 1: In this stage, we train an uplift model CAN-U to learn from the observational dataset $D = \{(x_i, t_i, y_i)\}_{i=1}^N$. CAN-U leverages the IPM loss function and propensity score prediction network to balance the representation distribution across different treatment groups. The training loss of CAN-U is defined as follows:

$$\min_{\theta} \max_{\pi} \mathcal{L}_{\theta} - \lambda \mathcal{L}_{\pi} \quad (3)$$

$$\mathcal{L}_{\theta} = \mathcal{L}(\hat{y}_i, y_i) + \alpha \mathcal{L}_{IPM_i} + \beta \mathcal{R}(h) \quad (4)$$

where \mathcal{L}_{θ} represents the training loss of outcome prediction, \mathcal{L}_{π} represents the training loss of the propensity score estimation network $\pi(t|\phi(X))$, $\phi(X)$ means the latent space representation of X , $\mathcal{L}(\hat{y}_i, y_i)$ represents the model's estimation error on factual outcome, \mathcal{L}_{IPM_i} is the IPM loss, and $\mathcal{R}(h)$ is the L2 regularization. λ, α, β denote the weight for adversarial task, IPM loss term and the L2 regularization, respectively, all of which are hyperparameters. We perform adversarial training on CAN-U via minimax bilevel optimization. Specifically, TSCAN first optimizes the parameters of the propensity score estimation network π to minimize the loss \mathcal{L}_{π} . Then, the model adjusts other parameters θ (including those of the encoder and outcome prediction network) to minimize \mathcal{L}_{θ} while maximizing \mathcal{L}_{π} . This adversarial process forces the encoder to eliminate treatment-related confounding factors from X , thereby indirectly aligning the latent space distributions between the treatment and control groups (through the IPM loss). Ultimately, this process enhances the robustness of individual causal effect estimation. The detailed model is shown in Section 4.2.

Stage 2: In this stage, we generate the counterfactual samples by transforming the observed treatment t_f of each sample either randomly or probabilistically into a counterfactual treatment t_{cf} ($t_{cf} \neq t_f$). This process results in a counterfactual dataset $(X, t_f, y_f) \rightarrow (X, t_{cf}, \emptyset)$, where " \rightarrow " denotes counterfactual sampling processes on the treatment and \emptyset represents the null outcome to be predicted. For example, if a merchant did not participate in a marketing activate in reality ($t_f=0$), the counterfactual scenario means that the merchant has conducted the activity ($t_{cf}=1$). Since the counterfactual outcomes are unobservable, we generate the pseudo uplift label \tilde{u} by CAN-U trained in Stage 1, where $\tilde{u} = \hat{y}_{cf} - \hat{y}_f$ and \hat{y} is the prediction result of CAN-U. As a result, we get a complete and balanced dataset $\tilde{D} = (X, t_f, y_f, t_{cf}, \tilde{u})$. Finally, CAN-D model is trained on \tilde{D} with the loss function:

$$\mathcal{L}_d = \mathcal{L}(y_f, \hat{y}_f^d) + \gamma \mathcal{L}(\tilde{u}, \hat{u}^d) \quad (5)$$

where \hat{y}_f^d is the factual outcome predicted by CAN-D, \hat{u}^d is the uplift prediction value generated by CAN-D, and γ is the weight assigned to the uplift prediction loss.

4.2 TSCAN

The network architecture of TSCAN is depicted in Figure 2. In contrast to CAN-U, IPM and propensity score prediction module are removed in CAN-D. Beyond this modification, no differences exist in structural aspects.

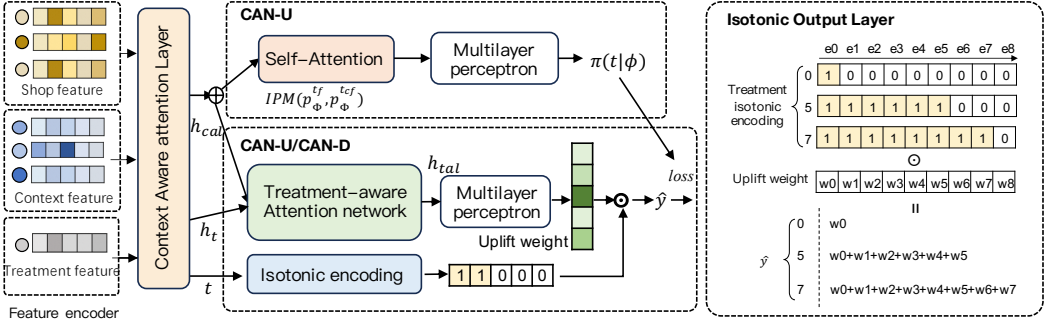


Fig. 2. The network architecture of CAN-U and CAN-D.

4.2.1 Feature encoder. For each merchant instance (X_i, t_i, y_i) , the feature encoder is used to encode both the features X_i (including context feature) and the treatment t_i into embeddings. Here, $X_i = (x_i^1, x_i^2, \dots, x_i^k, \dots, x_i^K)$, where k is the feature index and K represents the number of features. Specifically, for sparse features, the feature encoder performs a lookup operation in the corresponding embedding table $E_k^{cat} \in \mathbb{R}^{L,M}$ ($k \in \Omega^{cat}$), where Ω^{cat} is the set of sparse features, L is the predefined maximum number of categories, and M represents the embedding dimension. For continuous features k , where $k \in \Omega^{num}$, the feature value x^k is multiplied by the weight vector $\mathbf{w}_k \in \mathbb{R}^M$ and added to the bias vector $\mathbf{b}_k \in \mathbb{R}^D$, and Ω^{num} is the set of continuous features. This process aims to encode both the semantic and numerical information of the continuous features. Notably, the treatment feature t_i is encoded in the same manner as features X_i . The formulaic expression is as follows:

$$e_k = \begin{cases} E_k^{cat}(x^k), & \text{if } k \in \Omega^{cat} \\ \mathbf{w}_k * x^k + \mathbf{b}_k, & \text{if } k \in \Omega^{num} \end{cases} \quad (6)$$

Finally, we obtain the corresponding merchant embedding, context embedding, and treatment embedding $\{e_s, e_c, e_t\}_i$.

4.2.2 Context-Aware Attention Layer. In online food marketing scenarios, the contextual features (such as supply and demand status, location, area type, and time-related factors) of a merchant may affect the effectiveness of the treatments. For example, during peak meal hours, consumers may be less sensitive to merchant subsidies. Conversely, users will exhibit higher sensitivity to food prices during off-peak hours. To enable the model to capture the variations in treatment effects across different contexts, we propose a Context-Aware Attention Layer. This module facilitates feature interactions among the treatment, merchant and the context features. The network architecture is illustrated in the Figure 3. In Context-Aware Gate Attention, we dynamically extract the input

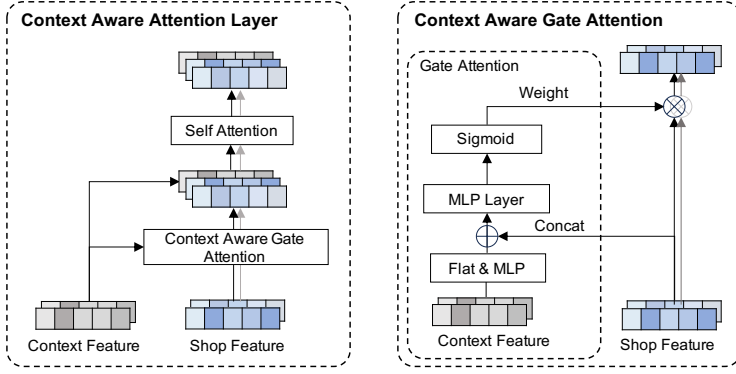


Fig. 3. The architecture of Context-Aware Attention Layer and the Context-Aware Gate Attention.

merchant features e_s according to the context information:

$$h_s = a_s e_s \quad (7)$$

where e_s denotes the merchant feature embeddings, a_s is the context-aware attention weights assigned to e_s , and h_s denotes the adaptive representation of the merchant. We apply the Gated Attention mechanism to extract merchant feature weights a_s under different contexts. The weight a_s is calculated as:

$$a_s = 1 + \sigma(W_p[e_s; \text{MLP}(\text{Flat}(e_c))] + b_p) \quad (8)$$

where e_c denotes the context features, W_p and b_p are the parameters of the MLP layer, ";" is the concatenation operator, and σ refers to the activation function. We flatten the encoded e_c and feed it into an MLP layer to aggregate all context features before calculating a_s . Finally, in the Context-Aware Attention Layer, we perform a self-attention operation on the context features e_c and h_s to facilitate interactions between the context and merchant features. The merchant embedding output by the Context-Aware Attention Layer can be expressed as:

$$h_{cal} = \text{Self-Attn}([h_s, e_c]) \quad (9)$$

where Self-Attn represents the self attention operation. In order to identify the treatment effectiveness in different contexts, we also perform Context-Aware Attention on the treatment features and context features. The resulting treatment embedding can be expressed as:

$$h_t = a_t e_t \quad (10)$$

$$a_t = 1 + \sigma(W_t[e_t; \text{MLP}(\text{Flat}(e_c))] + b_t) \quad (11)$$

4.2.3 Treatment-Aware Attention Network. This module is primarily used to capture the various responses of merchants across different treatment groups. First, we apply the Treatment-Aware Gate Attention to the input feature h_{cal} :

$$h_{tal} = \alpha_{tal} h_{cal} \quad (12)$$

$$\alpha_{tal} = 1 + \sigma(W_q[h_{cal}; h_t] + b_q) \quad (13)$$

where h_t is the treatment embedding output by Context-Aware Attention Layer, and W_q and b_q represent the gate attention parameters. Subsequently, the output of the Treatment-Aware Attention layer can be expressed as:

$$h_{tal} = \text{Self-Attn}([h_{tal}, h_t]) \quad (14)$$

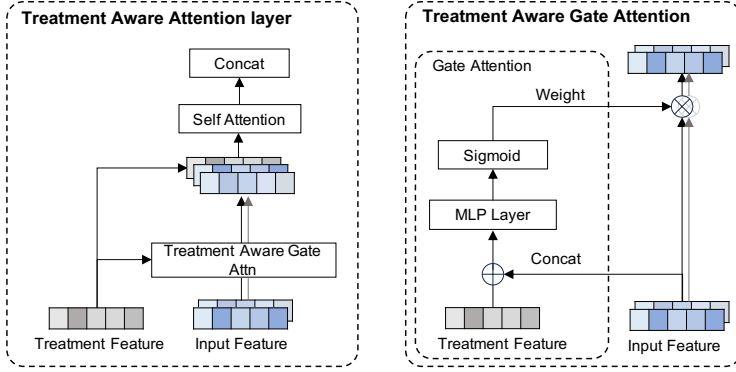


Fig. 4. The architecture of Treatment Aware Attention Layer and the Treatment Aware Gate Attention.

By dynamically weighting the features of merchants in different treatment groups, TSCAN can effectively identify the types of merchants that are more sensitive to treatments in each context, as well as the merchant or contextual characteristics that have a greater influence on the treatment effect. Figure 4 shows the detailed structure.

4.2.4 Representation Constraint Module. In real-world scenarios, estimating causal effects directly from observational data often encounters challenges related to the selection bias ($t \not\perp X$). To address this issue, referring to methods such as [13, 26], we introduce IPM loss to balance the distribution of the representation space within CAN-U. For binary treatment, IPM is utilized to minimize the distance between the distributions of $h_{cal}^{t=0}$ and $h_{cal}^{t=1}$. To extend this methodology to continuous treatments, we sort and split the samples into two parts according to treatment values within each batch. Subsequently, we compute the distribution distance between the top 50% and bottom 50% of these samples. The IPM loss can be formulated as:

$$\mathcal{L}_{IPM} = \sup_{\|f\|_{\mathcal{H}_k} \leq 1} \{ \mathbb{E}_{x \sim p_{t \in T_0}} [f(x)] - \mathbb{E}_{x \sim p_{t \in T_1}} [f(x)] \} \quad (15)$$

$$= \| \mu_w(p_{t \in T_0}) - \mu_w(p_{t \in T_1}) \|_{\mathcal{H}_k} \quad (16)$$

In this work, we employ the Maximum Mean Discrepancy (MMD) as the IPM loss.

To partial out the covariates that affect the treatment assignment but not affect the outcome, thereby eliminating nuisance covariates, we integrate a propensity score regularization $\pi(\cdot)$ into CAN-U. This approach accounts for selection bias by ensuring that $f_{\theta}(x, t)$ remains invariant under perturbations, thereby enhancing the robustness of the uplift model [6]. In this work, for both binary and continuous treatments, the propensity score prediction loss can be formulated as:

$$\mathcal{L}_{\pi} = \sum_{i=1}^n (t_i - \pi(\hat{t}_i | \phi(x_i)))^2 \quad (17)$$

4.2.5 Isotonic Output Layer. In CAN-U, the incorporation of treatment regularizations introduces a trade-off in information. Inevitably, this process discards certain information that can be useful for outcome prediction, potentially resulting in a decline in predictive accuracy. Training an additional model named CAN-D with no treatment regularizations to directly model the uplift is expected to solve this problem. CAN-D is trained on the generated complete dataset $(X, t_f, y_f, t_{cf}, \tilde{u})$. By reinforcing factual samples, the estimation error of the previous model is adaptively corrected by CAN-D. To directly model the uplift values of samples, we employ an isotonic neural network as

the output layer of our model. First, we perform isotonic encoding on the treatment value t . For binary treatment types, the encoding method is defined as follows:

$$\text{IE}(t_i) = \begin{cases} [1, 0], & t_i = 0 \\ [1, 1], & t_i = 1 \end{cases} \quad (18)$$

For continuous treatments, we divide the treatment value from the minimum to the maximum into $M + 1$ intervals with equal spacing or frequency. When the treatment value equals t , the elements with subscripts less than or equal to t in the isotonic encoding vector are set to 1, otherwise they are set to 0. The formula is as follows:

$$\text{IE}(t_i) = [1 \text{ if } (k \leq \bar{t}_i * N) \text{ else } 0 \text{ for } k \text{ in } 0..M] \quad (19)$$

where \bar{t}_i represents the normalized value of t . The isotonic encoding of the treatment is calculated as $\mathbf{o}_{t_i} = \text{IE}(t_i)$. After processing through an MLP, the model uses the fused sample encoding h_{tal} to generate an uplift weight vector \mathbf{w}_i , where $\mathbf{w}_i \in \mathbb{R}^{M+1}$. In essence, each element in \mathbf{w}_i represents the uplift resulting from each of the incremental level of treatment. Finally, the predicted outcome value \hat{y}_i^d for sample can be obtained by taking the element-wise product of \mathbf{w}_i and \mathbf{o}_{t_i} :

$$\hat{y}_i^d = \mathbf{w}_i \odot \mathbf{o}_{t_i} \quad (20)$$

where $\mathbf{w}_i = [v_{i,0}, v_{i,1}, \dots, v_{i,k}, \dots, v_{i,M}]$ and \odot denotes the element-wise product. Naturally, the sum of elements from $v_{i,k}$ to $v_{i,k+s}$ represents the uplift value when the treatment increases from k to $k + s$. Therefore, the prediction of uplift \hat{u}_i^d can be formulated as:

$$\hat{u}_i^d = \mathbf{w}_i \odot |\mathbf{o}_{t_{i,cf}} - \mathbf{o}_{t_{i,f}}| \quad (21)$$

The prediction process is depicted in Figure 5. The advantages of the Isotonic Output Layer are:

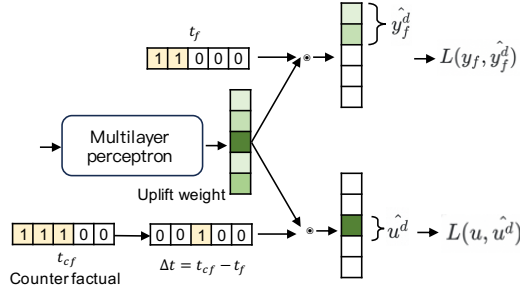


Fig. 5. An illustration of prediction process for the factual sample, counterfactual sample, and the corresponding uplift.

1. It allows TSCAN to directly model uplift, ensuring that the enhancement of uplift estimation minimally interferes with factual outcome prediction.

2. It maintains monotonicity. In most scenarios, such as online merchant diagnostics, ad recommendations, and coupon amount optimization, it is necessary to ensure that the effect of treatment on the outcome is monotonic. This requirement arises not only from the need to align with real-world behavior but also to enhance interpretability and reliability, which is especially crucial for earning the trust of business stakeholders when communicating the results. Isotonic neural networks can easily achieve this by squaring the weight vector of the isotonic neural network.

5 EMPIRICAL EVALUATIONS

In this section, we design and conduct a series of comprehensive experiments to address the following three research questions: RQ1: How does our TSCAN model perform compared to the baselines? RQ2: What is the contribution of each component in the model? RQ3: How does the TSCAN model perform in real-world online scenarios?

5.1 Experimental Setup

5.1.1 Datasets. We conduct experiments on two real-word datasets sourced from Ele.me, one of China's largest online food ordering platforms:

1) Eleshop-1M: this dataset contains online data of 1 million catering merchants, including features such as: shops ratings, operating hours, number of dishes, number of reviews, and context features such as business district type and regional user attributes. Based on Eleshop-1M, we predict a continuous treatment variable: the impact of shop rating on merchant order volume.

2) Shop Activities: this dataset includes data from 700k merchants, with 500k of them used for training and 200k reserved for testing. On this dataset, we predict a sparse treatment variable: the impact of participating in new customer activities on merchant order volume.

5.1.2 Evaluation Metrics. We evaluate the performance of TSCAN and other baseline models using two widely-recognized metrics: Normalized Area Under the Qini Curve (QINI) and Normalized Area Under the Uplift Curve (AUUC). QINI evaluates the effectiveness of uplift models in distinguishing between subsets of a population that respond differently to a treatment. AUUC provides a standardized performance measure that reflects the model's ability to accurately identify and segment the population based on their uplift potential. Additionally, in order to further evaluate the fitting capability of the model across different contexts, we propose two new metrics: Context-wise AUUC (CAUUC) and Context-wise QINI (CQINI). These two metrics extend AUUC and QINI by incorporating context-specific evaluations, and the calculations of them are formulated as:

1) CAUUC: CAUUC is the weighted average of AUUC for merchant groups across different contexts:

$$CAUUC = \frac{\sum_{g=1}^G N_g * AUUC_g}{\sum_{g=1}^G N_g} \quad (22)$$

where G is the number of merchant groups divided by different contexts, N_g is the sample count of group g , and $AUUC_g$ is the AUUC value of group g .

2) CQINI: CQINI is the weighted average of QINI for merchant groups across different contexts:

$$CQINI = \frac{\sum_{g=1}^G N_g * QINI_g}{\sum_{g=1}^G N_g} \quad (23)$$

where $QINI_g$ is the QINI value of group g . For continuous treatments, we discretize them into multiple intervals and compute the average AUUC and average QINI for each interval. The Gain Curve is a visualization tool used to evaluate the effectiveness of uplift models. It plots the cumulative uplift against the proportion of the population targeted, ranked by predicted uplift scores. A steeper Gain Curve indicates superior model performance, as it shows that the model can achieve higher uplift by targeting a smaller subset of the population.

5.1.3 Baselines and Parameter Settings. To evaluate the effectiveness of our model, we select a set of the most representative methods, including meta-learners (S-Learner and T-Learner), tree-based models (BART), and deep uplift models (TarNet, TransTEE, CFR-ISW, and EFIN). In the baseline models, context features and merchant features are input into the model together without any special processing. All models are implemented using Python 2.7 and PyTorch. We use the Adam

optimizer to train the models. To prevent overfitting during the early stages of training and to ensure stability, we employ a warm-up strategy for all methods. Specifically, we initially set the learning rate at 0.001 and gradually increase it to 0.015. The batch size is set to 256. The isotonic encoding size M is set to 128. The uplift prediction loss weight γ is set to 0.6. All experiments are repeated five times, and the results are averaged.

5.2 Overall Performance Assessment

5.2.1 *RQ1: How does our TSCAN model perform compared to the baseline models?* The performance of TSCAN compared with the baseline models on the datasets Eleshop-1M and Shop Activities is shown in Table 1. From the results, we can draw the following conclusions:

- 1) Most deep models outperform S-Learner and T-Learner, indicating that in complex merchant diagnosis scenarios, fully modeling interactions among merchant features, context features, and treatment features is essential. Complex network architectures are more adept at managing these interactions.
- 2) Compared to other baseline models, TSCAN exhibits a notable enhancement in performance. For instance, it achieves an AUUC increase of 0.0049 and a CAUUC increase of 0.0153 compared to TransTEE on the Eleshop-1M. These results validate the efficacy of our proposed two-stage training strategy and the context-aware network structure.
- 3) TSCAN achieves the best performance on both the Eleshop-1M and Shop Activities datasets. This indicates that TSCAN can effectively handle both continuous and binary treatments. It’s attributed to the isotonic output layer, which is designed to predict binary treatments with a 2-dimensional uplift weight vector and continuous treatments with an N-dimensional uplift weight vector.

To intuitively compare the cumulative uplift effects across different models, we present the Gain Curve of various approaches on the Eleshop-1M benchmark in Figure 6. In a Gain Curve, a steeper trajectory reaching higher uplift faster indicates better model performance. The ideal curve approaches the upper-left corner, while the diagonal (black dotted curve) represents random ordering. As shown in this figure, our analysis demonstrates that TSCAN (red curve) exhibits the steepest ascent among the compared models, confirming its enhanced capability to identify high-uplift individuals through effective causal effect prioritization.

Table 1. Model performance comparison on the two datasets

Dataset	Eleshop-1M				Shop Activities			
Metrics	CQINI	QINI	CAUUC	AUUC	CQINI	QINI	CAUUC	AUUC
S-Learner	0.1708	0.1836	0.6442	0.6649	0.0874	0.0828	0.5819	0.58
T-Learner	0.2026	0.2163	0.6751	0.6871	0.0881	0.0842	0.6106	0.5955
BART	0.1236	0.1615	0.6242	0.642	0.0914	0.0861	0.6196	0.6096
TarNet	0.2323	0.2248	0.7142	0.7079	0.0936	0.0969	0.6335	0.6283
TransTEE	0.2652	0.2608	0.7533	0.7489	0.0919	0.0935	0.627	0.6256
EFIN	0.2344	0.2267	0.7162	0.7107	0.0828	0.0837	0.5947	0.5949
CFR-ISW	0.2536	0.2489	0.7434	0.7388	0.0906	0.0925	0.6217	0.6167
TSCAN(ours)	0.2839	0.2687	0.7686	0.7538	0.0994	0.1054	0.6379	0.6328

5.2.2 *RQ2: What is the contribution of each component in the model?* To evaluate the effectiveness of the two-stage training strategy in the TSCAN model, we compare TSCAN (CAN-D) with the CAN-U model, which is produced in the first stage. Furthermore, to examine the impact of the Context-Aware attention layer and context features on model performance, we create two modified versions

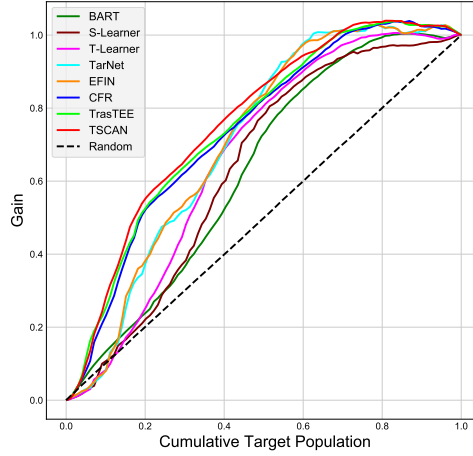


Fig. 6. The Gain Curve of models on Eleshop-1M benchmark.

of TSCAN, called TSCAN-RA and TSCAN-RC. Specifically, TSCAN-RA is setup by removing the Context-Aware attention layer from both sub-models of TSCAN and replacing it with a fully connected layer, treating context features as part of the merchant features. TSCAN-RC is developed by entirely excluding contextual features from the dataset to assess their contribution to treatment effect estimation. The experimental results are presented in Table 2. Based on the experimental results, the following conclusions can be established:

- 1) TSCAN (the CAN-D sub-model) outperforms CAN-U in all tasks, indicating that CAN-D can adaptively correct the errors generated by CAN-U. Though modeling the uplift value directly and separately, CAN-D is able to focus on the supervised learning of uplift labels while maintaining the accuracy of factual outcome prediction.
- 2) On both datasets, TSCAN significantly outperforms TSCAN-RC, suggesting that contextual features play a vital role in predicting treatment effects, and highlighting that the the same treatment can yield different outcomes depending on the context.
- 3) On both tasks, TSCAN outperforms TSCAN-RA (e.g., an AUUC improvement of 0.0182 on Eleshop-1M), indicating that the Context-Aware attention layer enables more effective modeling of the interactions among context, merchant, and treatment features.

Table 2. Model performance comparison of TSCAN-RC, TSCAN-RA, CAN-U and TSCAN (the CAN-D sub-model)

Dataset	Eleshop-1M				Shop Activities			
Metrics	CQINI	QINI	CAUUC	AUUC	CQINI	QINI	CAUUC	AUUC
TSCAN-RC	0.1737	0.1847	0.6536	0.6682	0.865	0.0812	0.5812	0.5735
TSCAN-RA	0.2526	0.2429	0.738	0.7334	0.0939	0.0972	0.6234	0.6302
CAN-U	0.2639	0.2536	0.7474	0.743	0.0941	0.0977	0.6283	0.6309
TSCAN(CAN-D)	0.2839	0.2687	0.7686	0.7538	0.0994	0.1054	0.6379	0.6328

To study the impact of the uplift prediction loss weight γ for on the CAN-D model, we also conduct comparative experiments with different γ values, using AUUC and CAUUC as the primary

evaluation metrics. The experimental results are shown in Figure 7. It is observed that both the AUUC and CAUUC metrics exhibit an initial increase followed by a subsequent decline when the γ value varies between 0.5 and 0.8. The optimal γ value is approximately 0.6, at which point the AUUC reaches 0.6328 and the CAUUC attains 0.6379. The black dotted line represents the performance of CAN-U (AUUC: 0.6309, CAUUC: 0.6283). It can be concluded that when γ is equal to 0.6, the CAN-D model achieves an improvement of 0.0019 (0.3%) in AUUC and 0.0096 (1.5%) in CAUUC compared to CAN-U. This demonstrates that the two-stage training strategy enhances the model's counterfactual prediction accuracy and its ability to process contextually effectively.

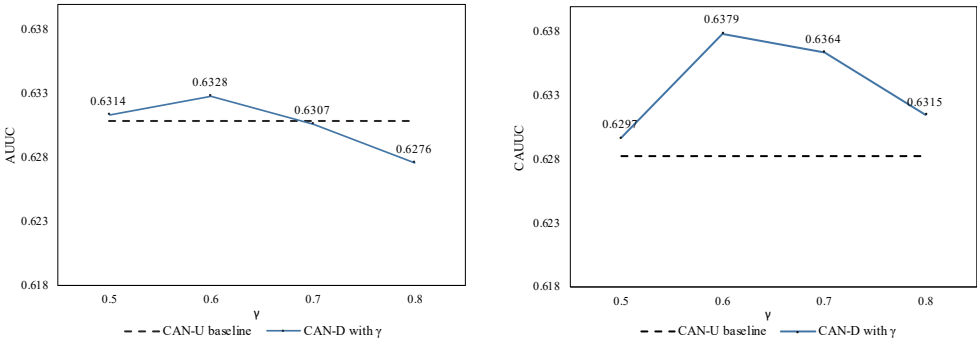


Fig. 7. The CAN-D performance on different prediction loss weight γ

5.2.3 RQ3: How does the TSCAN model perform in real-world online scenarios? To evaluate the performance of our model in real-world online scenarios, we have deployed TSCAN in the merchant diagnosis context of Ele.me, a leading online food ordering platform in China. In this application, we estimate the increase in order counts (outcome) after the merchant adopts specific suggestions, such as configuring a 2-yuan red envelope for new customers and setting up shop posters. Based on these estimates we provide merchants with the most effective suggestions with a high potential adoption rate. Our work focuses on improving the performance of the uplift model. We verify the performance of our model by online A/B experiments. We collect the order results from two groups of shops after adopting the suggestions generated by different models. As shown in Table 3, in the online experiment, our proposed model outperforms the baseline model BART, achieving a 0.76% increase in orders, a AUUC improvement of 0.0349, and a CAUUC improvement of 0.0411.

Table 3. Online performance comparison of our TSCAN and baseline model BART

Metrics	CAUUC	AUUC	Order increase
BART	-	-	-
TSCAN	0.0411	0.0349	0.76%

6 Conclusion

In this paper, we introduce TSCAN, a Context-Aware uplift model based on a two-stage training approach. TSCAN effectively mitigates the negative impacts of traditional regularization methods like IPM loss and propensity score prediction, by employing a two-stage training strategy with

CAN-U and CAN-D models. Additionally, by integrating a Context-Aware attention layer, TSCAN leverages contextual features to enhance the accuracy of treatment effect estimations across diverse environments. Experimental evaluations on two real-world datasets demonstrate TSCAN's superior performance compared to existing baseline models. Furthermore, its deployment on an online platform resulted in significant improvements in merchant operation diagnostics. Future work will focus on developing end-to-end training methodologies and exploring more generalized mechanisms for contextual information interaction to further enhance uplift modeling capabilities.

References

- [1] Business of Apps. 2024. Food Delivery App Revenue and Usage Statistics. Website. <https://www.businessofapps.com/data/food-delivery-app-market/>.
- [2] Shanqi Zhang, Hui Luan, Feng Zhen, Yu Kong, and Guangliang Xi. 2023. Does online food delivery improve the equity of food accessibility? A case study of Nanjing, China. *Journal of Transport Geography* 107 (2023), 103516. doi:10.1016/j.jtrangeo.2022.103516
- [3] Xu Ji, Xuerong Li, and Shouyang Wang. 2024. Balance between profit and fairness: Regulation of online food delivery OFD platforms. *International Journal of Production Economics* 269 (2024), 109144. doi:10.1016/j.ijpe.2024.109144
- [4] Liuyi Yao, Zhixuan Chu, Sheng Li, Yaliang Li, Jing Gao, and Aidong Zhang. 2021. A Survey on Causal Inference. *ACM Trans. Knowl. Discov. Data* 15, 5, Article 74 (May 2021), 46 pages. doi:10.1145/3444944
- [5] Weijia Zhang, Jiuyong Li, and Lin Liu. 2021. A unified survey of treatment effect heterogeneity modeling and uplift modeling. arXiv:2007.12769 [stat.ME] <https://arxiv.org/abs/2007.12769>
- [6] Yi-Fan Zhang, Hanlin Zhang, Zachary Chase Lipton, Li Erran Li, and Eric P. Xing. 2022. Exploring Transformer Backbones for Heterogeneous Treatment Effect Estimation. *Trans. Mach. Learn. Res.* 2023 (2022). <https://api.semanticscholar.org/CorpusID:249151761>
- [7] Liuyi Yao, Zhixuan Chu, Sheng Li, Yaliang Li, Jing Gao, and Aidong Zhang. 2021. A Survey on Causal Inference. *ACM Trans. Knowl. Discov. Data* 15, 5, Article 74 (May 2021), 46 pages. doi:10.1145/3444944
- [8] Zongyu Li, Zheng Hua Zhu, Xiaoning Guo, Shuai Zheng, Zhenyu Guo, Siwei Qiang, and Yao Zhao. 2022. A survey of deep causal models and their industrial applications. *Artif. Intell. Rev.* 57 (2022), 298. <https://api.semanticscholar.org/CorpusID:253523500>
- [9] Sören R. Künzel, Jasjeet S. Sekhon, Peter J. Bickel, and Bin Yu. 2019. Metalearners for estimating heterogeneous treatment effects using machine learning. *Proceedings of the National Academy of Sciences* 116, 10 (Feb. 2019), 4156–4165. doi:10.1073/pnas.1804597116
- [10] Hugh A. Chipman, Edward I. George, and Robert E. McCulloch. 2010. BART: Bayesian additive regression trees. *The Annals of Applied Statistics* 4, 1 (March 2010). doi:10.1214/09-aoas285
- [11] Vikas Ramachandra, Susan Athey, and Stefan Wager. 2015. Estimation and Inference of Heterogeneous Treatment Effects using Random Forests. *J. Amer. Statist. Assoc.* 113 (10 2015). doi:10.1080/01621459.2017.1319839
- [12] Christos Louizos, Uri Shalit, Joris M. Mooij, David A. Sontag, Richard S. Zemel, and Max Welling. 2017. Causal Effect Inference with Deep Latent-Variable Models. In *Neural Information Processing Systems*. <https://api.semanticscholar.org/CorpusID:260564>
- [13] Negar Hassanpour and Russell Greiner. 2019. Counterfactual Regression with Importance Sampling Weights. In *Proceedings of the Twenty-Eighth International Joint Conference on Artificial Intelligence, IJCAI-19*. International Joint Conferences on Artificial Intelligence Organization, 5880–5887. doi:10.24963/ijcai.2019/815
- [14] Dugang Liu, Xing Tang, Han Gao, Fuyuan Lyu, and Xiuqiang He. 2023. Explicit Feature Interaction-aware Uplift Network for Online Marketing. In *Proceedings of the 29th ACM SIGKDD Conference on Knowledge Discovery and Data Mining (Long Beach, CA, USA) (KDD '23)*. Association for Computing Machinery, New York, NY, USA, 4507–4515. doi:10.1145/3580305.3599820
- [15] Ruqi Liu, Changchang Yin, and Ping Zhang. 2020. Estimating Individual Treatment Effects with Time-Varying Confounders. In *2020 IEEE International Conference on Data Mining ICDM*. 382–391. doi:10.1109/ICDM50108.2020.00047
- [16] Fredrik D. Johansson, Uri Shalit, and David Sontag. 2016. Learning representations for counterfactual inference. In *Proceedings of the 33rd International Conference on International Conference on Machine Learning - Volume 48 (New York, NY, USA) (ICML '16, Vol. 48)*. JMLR.org, New York, New York, USA, 3020–3029.
- [17] Claudia Shi, David M. Blei, and Victor Veitch. 2019. *Adapting neural networks for the estimation of treatment effects*. Curran Associates Inc., Red Hook, NY, USA.
- [18] Changhee Lee, Nicholas Mastronarde, and Mihaela van der Schaar. 2018. Estimation of Individual Treatment Effect in Latent Confounder Models via Adversarial Learning. arXiv abs/1811.08943 (2018). <https://api.semanticscholar.org/CorpusID:53716914>

- [19] Jinsung Yoon, James Jordon, and Mihaela van der Schaar. 2018. GANITE: Estimation of Individualized Treatment Effects using Generative Adversarial Nets. In *6th International Conference on Learning Representations, ICLR 2018, Vancouver, BC, Canada, April 30 - May 3, 2018, Conference Track Proceedings*. OpenReview.net. <https://openreview.net/forum?id=ByKWUeWA->
- [20] Ioana Bica, James Jordon, and Mihaela van der Schaar. 2020. Estimating the effects of continuous-valued interventions using generative adversarial networks. In *Proceedings of the 34th International Conference on Neural Information Processing Systems (Vancouver, BC, Canada) (NIPS '20)*. Curran Associates Inc., Red Hook, NY, USA, Article 1379, 12 pages.
- [21] Uri Shalit, Fredrik D. Johansson, and David Sontag. 2017. Estimating individual treatment effect: generalization bounds and algorithms. In *Proceedings of the 34th International Conference on Machine Learning - Volume 70 (Sydney, NSW, Australia) (ICML '17)*. JMLR.org, 3076–3085.
- [22] Insung Kong, Yuha Park, Joonhyuk Jung, Kwonsang Lee, and Yongdai Kim. 2023. Covariate balancing using the integral probability metric for causal inference. 17430–17461 pages. arXiv:2305.13715 [stat.ML] <https://arxiv.org/abs/2305.13715>
- [23] Tobias Hatt and Stefan Feuerriegel. 2021. Estimating Average Treatment Effects via Orthogonal Regularization. In *Proceedings of the 30th ACM International Conference on Information & Knowledge Management (Virtual Event, Queensland, Australia) (CIKM '21)*. Association for Computing Machinery, New York, NY, USA, 680–689. doi:10.1145/3459637.3482339
- [24] Anpeng Wu, Kun Kuang, Junkun Yuan, Bo Li, Pan Zhou, Jianrong Tao, Qiang Zhu, Yueting Zhuang, and Fei Wu. 2020. Learning Decomposed Representation for Counterfactual Inference. *ArXiv abs/2006.07040* (2020). <https://api.semanticscholar.org/CorpusID:219636246>
- [25] Jing Ma, Ruocheng Guo, Aidong Zhang, and Jundong Li. 2021. Multi-Cause Effect Estimation with Disentangled Confounder Representation. In *Proceedings of the Thirtieth International Joint Conference on Artificial Intelligence, IJCAI-21, Zhi-Hua Zhou (Ed.)*. International Joint Conferences on Artificial Intelligence Organization, 2790–2796. doi:10.24963/ijcai.2021/384 Main Track.
- [26] Serge Assaad, Shuxi Zeng, Chenyang Tao, Shounak Datta, Nikhil Mehta, Ricardo Henao, Fan Li, and Lawrence Carin. 2020. Counterfactual Representation Learning with Balancing Weights. *ArXiv abs/2010.12618* (2020). <https://api.semanticscholar.org/CorpusID:225067078>
- [27] Ahmed Alaa and Mihaela van der Schaar. 2018. Limits of Estimating Heterogeneous Treatment Effects: Guidelines for Practical Algorithm Design. In *Proceedings of the 35th International Conference on Machine Learning (Proceedings of Machine Learning Research, Vol. 80)*, Jennifer Dy and Andreas Krause (Eds.). PMLR, 129–138. <https://proceedings.mlr.press/v80/aaa18a.html>
- [28] Fredrik Johansson, Nathan Kallus, Uri Shalit, and David Sontag. 2018. Learning Weighted Representations for Generalization Across Designs. *arXiv: Machine Learning* (02 2018). doi:10.48550/arXiv.1802.08598
- [29] Xing Wu, Shaoqi Peng, Jingwen Li, Jian Zhang, Qun Sun, Weimin Li, Quan Qian, Yue Liu, and Yike Guo. 2024. Causal inference in the medical domain: a survey. *Applied Intelligence* 54, 6 (April 2024), 4911–4934. doi:10.1007/s10489-024-05338-9
- [30] Hal R. Varian. 2016. Causal inference in economics and marketing. *Proceedings of the National Academy of Sciences* 113, 27 (2016), 7310–7315. doi:10.1073/pnas.1510479113 arXiv:<https://www.pnas.org/doi/pdf/10.1073/pnas.1510479113>
- [31] Andrew Forney and Scott Mueller. 2022. Causal inference in AI education: A primer. *Journal of Causal Inference* 10, 1 (2022), 141–173. doi:10.1515/jci-2021-0048
- [32] Qiang Huang, Jing Ma, Jundong Li, Ruocheng Guo, Huiyan Sun, and Yi Chang. 2023. Modeling Interference for Individual Treatment Effect Estimation from Networked Observational Data. *ACM Trans. Knowl. Discov. Data* 18, 3, Article 48 (Dec. 2023), 21 pages. doi:10.1145/3628449
- [33] Kai Lagemann, Christian Lagemann, Bernd Taschler, and Sach Mukherjee. 2023. Deep learning of causal structures in high dimensions under data limitations. *Nature Machine Intelligence* 5, 11 (2023), 1306–1316. doi:10.1038/s42256-023-00744-z
- [34] Kaixiang Lin, Jianpeng Xu, Inci M. Baytas, Shuiwang Ji, and Jiayu Zhou. 2016. Multi-Task Feature Interaction Learning. In *Proceedings of the 22nd ACM SIGKDD International Conference on Knowledge Discovery and Data Mining (San Francisco, California, USA) (KDD '16)*. Association for Computing Machinery, New York, NY, USA, 1735–1744. doi:10.1145/2939672.2939834
- [35] Chenhui Xu, FUXUN YU, Maoliang Li, Zihao Zheng, Zirui Xu, Jinjun Xiong, and Xiang Chen. 2024. Infinite-Dimensional Feature Interaction. In *Advances in Neural Information Processing Systems*, A. Globerson, L. Mackey, D. Belgrave, A. Fan, U. Paquet, J. Tomczak, and C. Zhang (Eds.), Vol. 37. Curran Associates, Inc., 92381–92400. https://proceedings.neurips.cc/paper_files/paper/2024/file/a7efd7734bb2e79997f8d1137ece3f09-Paper-Conference.pdf
- [36] Kshitij Goyal, Sebastijan Dumancic, and Hendrik Blockeel. 2020. Feature Interactions in XGBoost. (2020). doi:10.48550/arXiv.2007.05758 arXiv:2007.05758 [cs.LG]